Constant Fluidic Mass Control for Soft Actuators Using Artificial Neural Network Algorithm

Heng Xu[1,2], Priyanshu Agarwal[2], and Benjamin Stephens-Fripp*[2]

***Abstract*— Soft fluidic actuators are increasingly being used for wearable haptic devices due to their high energy density and low encumbrance. These actuators are typically controlled using constant fluidic pressure control (CFPC), where the actuator pressure is switched between a high pressure source and atmospheric pressure using a fluidic valve. However, this type of control has several limitations for soft actuators including limited dynamic range, slow actuator response, low pressure control resolution and unnatural haptic interaction. In this paper, we present a novel control strategy for soft fluidic actuators, called constant fluidic mass control (CFMC), where the mass of fluid introduced into the actuator is kept constant during actuation, rather than the pressure as in CFPC. Our experimental results show that compared to CFPC, CFMC results in a larger dynamic range of actuator output forces, faster actuator response time to reach a desired target pressure, and higher resolution of pressure control, which makes it particularly useful for wearable haptics. In addition, CFMC enables analog pressure control and we present a neural-network-based supervised learning algorithm for accurate pressure control of soft actuators. Results show that our algorithm can predict actuator pressure with an accuracy of 99% and can be generalized to different soft TPU-fabric fluidic actuators.**

I. Introduction

Soft actuators are increasingly becoming popular in the field of robotics and wearable haptics because of their better contact compliance and lower weight and encumbrance than their rigid counterparts. Different energy sources have been explored in literature to power these soft actuators, including fluidic actuation [1], electrostatic actuation [2], electromagnetic actuation [3], and thermal actuation [4]. Due to their high energy density and low encumbrance, soft fluidic actuators are widely used for wearable devices [1], [5]–[7]. Primarily constant fluidic pressure control (CFPC) has been explored in the literature to control these soft actuators [1], [8]–[11]. This control approach uses a simple actuation structure (one discrete valve per actuator) and a binary (on-off) control mechanism, which allows the actuator pressure to track the fluidic source pressure under a dynamic load. However, as a result, CFPC has several limitations: (1) Limited dynamic range: Dynamic range of the force offered by a soft actuator is limited and governed by only its operational pressure, since the actuator pressure can only switch between source and atmospheric pressures. (2) Slow actuator response: Inflation and deflation response time of a soft actuator is determined by the source pressure and cannot be independently modulated. (3) Low pressure control resolution: Only binary control of actuator pressure is achievable with this type of control. (4) Unnatural haptic interaction: Only active or exogenous control of actuator pressure is possible and it is not inherently tied to how the user interacts with the actuator, which leads to unnatural haptic interaction.

To address these limitations, we propose constant fluidic mass control (CFMC), where a constant mass of fluid is trapped inside the actuator. As the user interacts with the actuator, any change in actuator pressure due to this interaction further contributes to improving the haptic interaction. Unlike previous work in the literature for soft hand control [12], which uses pressure sensors and first-principles models to estimate the fluidic mass, we regulate the fluidic mass by accurately controlling the timing of the valves and trap it inside the actuator.

Analog pressure control using CFMC requires a reliable model of the overall fluidic system including the actuator. Some researchers have developed first-principles based theoretical models to predict actuator behavior [13]–[17]. However, these models could only approximate the actuator behavior for a limited set of inputs and cannot reliably capture all the nonlinearities in the fluidic system and are therefore difficult to generalize for different soft actuators.

In this work, we present a novel control approach (CFMC) of fluidic actuators for wearable haptics. Our approach allows for larger dynamic range, faster response time, and analog pressure control of soft actuators and also results in more natural haptic interaction. We implement a fluidic system to demonstrate the CFMC approach, and use this system to conduct experiments with soft actuators. Furthermore, we propose a neural-network-based supervised learning algorithm to enable analog pressure control of soft actuators using CFMC that can be generalized to new actuators. Our experiments comparing CFMC with CFPC approach demonstrate that CFMC can increase the dynamic range of soft actuators, reduce their response time to achieve a desired pressure, and enable analog pressure control, thereby providing more natural haptic feedback.

II. Methods

Fig. 1 shows the fluidic implementation of CFPC and CFMC. The fundamental difference between these two implementations is that in CFPC the actuator pressure can only exist in either the source or atmospheric pressure (ATM) state, whereas in CFMC the actuator can be disconnected from both the source and the atmosphere and therefore, hold a state different from both the source and the atmosphere.

[1]Department of Mechanical Engineering, Northwestern University, Evanston, IL, USA 60208
[2]Facebook Reality Labs, Redmond, WA, USA 98052
*E-mail: bensfripp@fb.com

CFPC uses a three-way valve such that the actuator is either connected to a compressed air source or ATM/vacuum by modulating this valve (Fig. 1(a)). CFMC, on the other hand, employs two three-way valves–a supply valve to control the intake of the pressurized air and an exhaust valve to control the exhaust to the ATM (Fig. 1(b)). CFMC then modulates the fluidic mass inside the actuator by changing the on/off time of the two valves based on the fluidic source pressure and initial actuator pressure. CFMC can also be implemented using two two-way valves. A three-way valve implementation is chosen here because those valves were readily available.

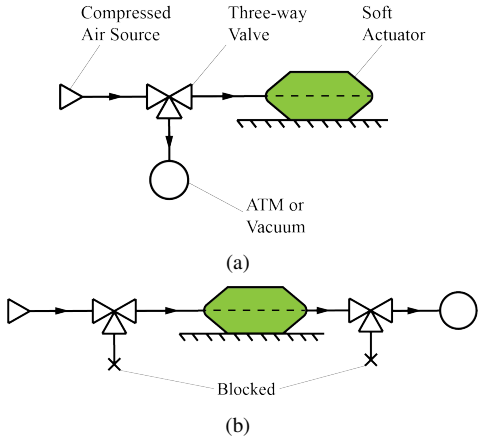

Fig. 1. Physical setup used for the alternate control methods used with pneumatic actuators. (a) CFPC valve arrangement; and, (b) CFMC valve arrangement.

A. CFMC Overview

Fig. 2 shows the principle illustration of how CFMC is particularly useful in haptics. The initial pressure and volume of the soft bladder are denoted as P_0 and V_0, respectively. As a finger interacts with the bladder, the pressure and volume of the bladder becomes P_1 and V_1, respectively. Assuming that the system follows an ideal gas law under isothermal condition, which for a closed system implies:

$$P_0 \times V_0 = P_1 \times V_1 \tag{1}$$

$$P_0 \times V_0 = (P_0 + \Delta P) \times (V_1 + \Delta V) \tag{2}$$

Assuming $\Delta P \times \Delta V \approx 0$, Eq. 2 is simplified to:

$$\Delta P = -\Delta V \times P_0/V_0 \tag{3}$$

In CFPC, the bladder volume decreases to V_1 as the finger interacts with it. As the pressure starts to increase as a result of this interaction (Eq. 3), the fluidic path of the actuator remains open to the constant pressure fluidic source, resulting in the actuator pressure remaining constant (P_0) at the source pressure.

In CFMC, as the finger interacts with the bladder, the bladder volume decreases, which results in an increase in air pressure (Eq. 3). However, since the air is trapped inside the actuator and the fluidic path from the actuator to the regulator is blocked, the increase in pressure is directly proportional to the reduction in volume and inversely proportional to the initial actuator volume. When we ignore the difference of contact area between CFPC and CFMC, the difference of interaction force between CFPC and CFMC will depend on the difference of the corresponding actuator pressure. Thus, the dynamic range of forces achievable using CFMC is also larger than CFPC.

Another advantage of CFMC is that it provides the ability to reduce the inflation time of the actuator by allowing for source pressures higher than the operational pressure of the actuator. On the other hand, in CFPC the source pressure is determined by the operational pressure of the actuator. Furthermore, unlike CFPC that only enables binary control of actuator pressure, CFMC allows for more precise analog pressure control of soft actuators. However, since the capacitance of soft actuators is typically nonlinear and there are many other nonlinearities in the fluidic system that are hard to capture using a first-principles model in a generalized manner, we use a neural-network-based supervised learning algorithm to achieve analog pressure control using CFMC. For example, quadratic relationship between pressure differential and flow for a pneumatic capacitor with compressible fluid, contribution of actuator material nonlinear force-displacement behavior to fluidic capacitance, distributed resistance and capacitance of fluidic tubing and flow choking at high pressure differential are some of the non-linearities present in pneumatic systems [15].

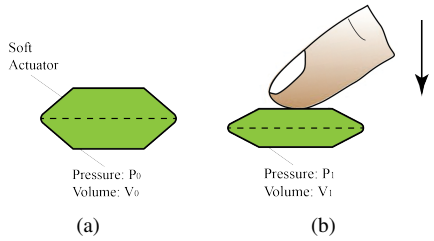

Fig. 2. Principle illustration of CFMC. (a) Initial actuator state. P_0 and V_0 are the initial pressure and volume of the soft bladder respectively; and, (b) Actuator state during interaction with finger. P_1 and V_1 are the pressure and volume of the bladder, after a finger interacts with the bladder.

B. Artificial Neural Network Control

To enable analog pressure control using CFMC, a neural-network-based algorithm was designed to predict the air pressure of the actuator, which is based on a method previously used to solve the inverse statics of non-constant curvature soft manipulators [18]. Fig. 3 shows the architecture of the feed-forward neural network and we used backpropagation to learn the weights of the network. To decrease the computation time and avoid potential overfitting issues, only one hidden layer was used in this algorithm. Since the air pressure of the actuator is modeled as a function of air source pressure, initial actuator pressure, and pressurizing/depressurizing time, the input layer has three corresponding neurons and a bias node. The neuron in the output layer is the final pressure of the actuator.

Five-fold cross-validation was used to train and evaluate the neural network algorithm. Two nonlinear activation functions (sigmoid function and hyperbolic tangent function) were tested in the preliminary experiments, in which the hyperbolic tangent function showed a faster convergence than the sigmoid function and therefore, we chose hyperbolic tangent function as the activation function for the final implementation. The other parameters in the algorithm are the learning rate and two early-stopping criterions (the minimum sum of squared error and the maximum number of epochs). The learning rate and the minimum sum of squared error were chosen as 0.05 and 0.01, respectively. The number of neurons in the hidden layer and the maximum number of epochs were also optimized.

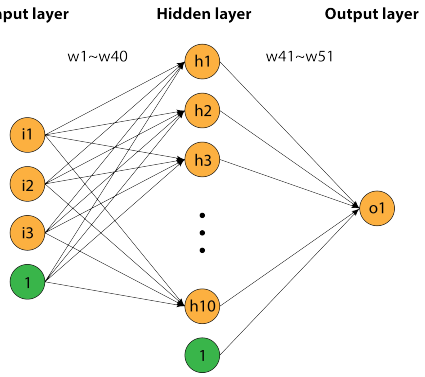

Fig. 3. Architecture of the feed-forward neural network with backpropagation for the constant fluidic mass control.

III. Experiments

We conducted two experiments using the same experimental setup to compare CFMC with CFPC. Experiment 1 compared the dynamic range of the actuator pressure between CFMC and CFPC, and the reaction force generated by the actuator during interaction. Experiment 2 investigated inflation/deflation response time and analog pressure control of a soft actuator based on a learned neural network model using CFMC. Two customized soft-fluidic-actuators with different capacitances were used for these experiments (Fig. 6), which represents a wide range of capacitances we would see in most haptics applications. These actuators were prototyped by heat sealing Nylon-backed TPU-fabric (Heat Sealable Coated Nylon Taffeta, Seattle Fabrics Inc.) to develop inflatable bladders. For the smaller actuator, a soft EPDM rubber tubing was also heat sealed during the fabric heat sealing process. For the larger actuator, a Nylon tubing was screwed on to a vented flat head screw to achieve an airtight connection. The soft actuator with a small capacitance (Fig. 6(a)) was used for experiments 1 and 2, and the larger capacitance soft actuator (Fig. 6(b)) was used to examine the generalization of our control approach.

A. Experiment Setup

The experiment setup (Fig. 4) consists of pneumatic and electric control as shown in the blue and red blocks, respectively.

The compressed air passes through a pneumatic filter (F03-02-000, Wilkerson Corporation) before being controlled by the valves (X-Valve, Parker-Hannifin Corporation). The valves modulate the pneumatic flow, which can either pressurize the soft actuator from the compressed air source, or depressurize the actuator to the ATM. The air source pressure for both CFMC and CFPC was adjusted by a pressure regulator (ControlAir Inc., 700-BD). Two three-way discrete valves were used to execute the CFMC, in which three different operations were carried out by turning on or off the two valves (Fig. 5): pressurization of the actuator, trapping the compressed air inside the actuator, and depressurization of the actuator. For the CFPC, we kept the pneumatic flow to the actuator connected to the compressed air source by turning on the primary valve and turning off the secondary valve (Fig. 5(a)).

Additionally, three pressure sensors (SSC-MANN060PG2A3, Honeywell International Inc.) were integrated into the setup to measure the pressure of the air source (between the blocks of "Air Filter" and "Valves' in Fig. 4), the actuator (between the blocks of "Valves" and "Actuators" in Fig. 4), and the depressurized outlet (between the blocks of "Valves" and "ATM" in Fig. 4). The microcontroller (PIC32, Microchip Technology Inc.) sent control signals to the valve driver based on the commands from PC and data from pressure sensors. The electric control loop was executed at 10 kHz, and pressure data from the three sensors was sampled at 10 kHz.

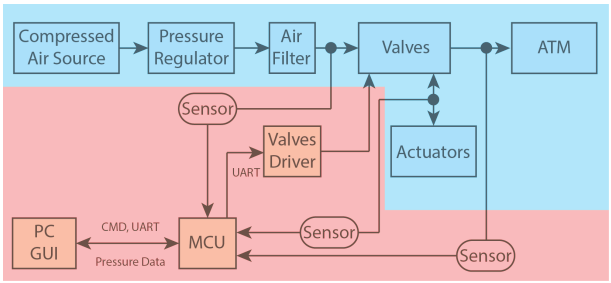

Fig. 4. Diagram of the experiment setup.

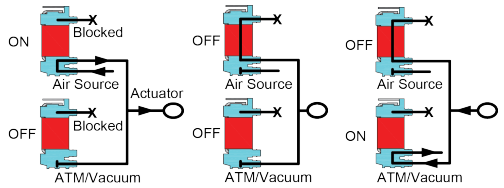

Fig. 5. Valves operation for constant fluidic mass control. (a) Pressurization of the actuator by turning the supply valve on and turning the exhaust valve off; (b) Holding the fluidic mass inside the actuator when turning off both the valves; and, (c) Depressurization of the actuator by turning the primary valve off and turning the secondary valve on.

B. Experiment Protocol

1) Experiment 1: Dynamic Force Response: During the experiment, an 8 mm diameter force sensor (CS8-10N,

SingleTact) was attached at the bottom of a flat acrylic block, which was used to press on the actuator to measure the reaction force offered by it (Fig. 7). The actuator was randomly controlled using CFMC or CFPC and the participant wore noise-canceling headphones playing a pink noise during the experiment to remove any bias based on the valve clicking sound for each type of control. The participant was presented with a total of 20 random trials (10 CFMC and 10 CFPC). In each trial, the participant was asked to keep the pressing force on the actuator as vertical as possible. These sets of trials were repeated three times. Each pressing took place after the participant was notified by a LED indicating the fully inflated actuator. Measurements from the three pressure sensors and the force sensor were sampled for 5 seconds at 10 kHz. The peak reaction force during the dynamic interaction was defined as the average force over the 100 millisecond period around the peak force during each pressing.

2) Experiment 2: Response Time and Analog Pressure Control: In this experiment, the final actuator pressure ($P_{actuator}$) is modeled as a function of air source pressure (P_{source}), initial actuator pressure ($P_{initial}$), and supply/exhaust valve on-time ($t_{execution}$), as shown in Eq. 4, using a neural network. While pressurizing the actuator, $t_{execution}$ is the on-time of the supply valve and while depressurizing, $t_{execution}$ is the on-time of the exhaust valve.

$$P_{actuator} = f(P_{source}, P_{initial}, t_{execution}) \tag{4}$$

Eight levels of the air source pressure were chosen as: 3.2, 4.7, 5.8, 6.7, 7.4, 8.5, 9.1, and 10.8 psi. Fifteen levels of pressurizing time (T_i) were chosen from 0 to 150 milliseconds with equidistant logarithmic intervals. Since 150 milliseconds was long enough for this actuator to be pressurized to the air source pressure, the initial actuator pressure was ranged from the atmosphere to the air source pressure. The inflation/deflation time (T_p) also had 15 levels from 3 milliseconds to 150 milliseconds with equidistant logarithmic intervals.

Preliminary experiments showed that the final actuator pressure was very consistent when the air source pressure, the initial actuator pressure, and the inflation/deflation times were fixed. Thus, the experiment with the same parameters was executed once. There were 450 trials ($15 * 15 * 2$) for each air source pressure in total (including pressurizing and depressurizing experiments). In each trial, measurements from the three pressure sensors were sampled at 10 kHz for 300 milliseconds, which was long enough for the actuator to reach the source pressure from atmospheric pressures and enter into a steady state.

Based on the neural network algorithm, three functions were trained for the actuator with a small capacitance (Fig. 6(a)):

- Actuator pressure as a function of supply/exhaust valve on-time only;
- Actuator pressure as a function of initial actuator pressure, supply valve on-time, and air source pressure (only for the pressurizing process);
- Actuator pressure as a function of initial actuator pressure and supply valve on-time for a specific air source pressure (10.8 psi) or exhaust valve on-time for a specific depressurized outlet (ATM).

The first function was used to investigate the ability of the neural network algorithm to learn the equivalent capacitance of the soft actuator. The second function studied the comprehensive impacts of potential variables (initial actuator pressure, supply valve on-time, and air source pressure) on the actuator pressure. Finally, since the source pressure is typically fixed and only modulate the initial actuator pressure and the pressurizing/depressurizing time, a third function was trained where the actuator pressure is a function of only the initial actuator pressure and the pressurizing/depressurizing time. In addition, the generalization of our approach was evaluated by repeating the process with another actuator with a much larger capacitance.

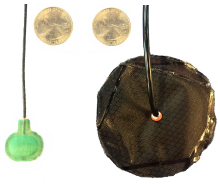

(a) (b)

Fig. 6. Two soft fluidic actuators used. (a) Small capacitance actuator for experiments 1 and 2; and, (b) Large capacitance actuator for testing generalization of approach.

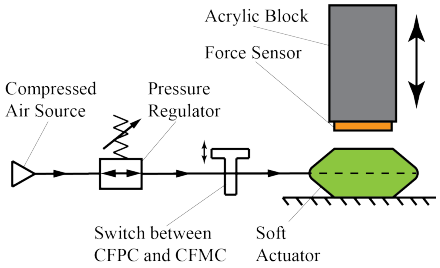

Fig. 7. Experiment 2 setup for measuring dynamic force.

IV. Results

A. Experiment 1: Larger Dynamic Range

When an actuator is pressurized, in CFPC the air is contained between a closed valve and a pressure regulator, whereas in CFMC the air is instead contained between two closed valves. In both setups, as you press the actuator the pressure increases occur based on Eq. 3. With CFPC, the regulator releases this additional pressure, but due to the slow mechanical response of the pressure regulator, some variation in pressure in the CFPC is observed in Fig. 8. For CFMC, however, becaused the air is contained between two closed valves, this additional pressure cannot escape (shown in Fig. 8) which results in a higher reaction force on the finger as a result, as shown in Fig. 9. The dynamic pressure range using

CFMC is 43% (3.2 psi, red curves in Fig. 8) as opposed to only 4% (0.3 psi, blue curves in Fig. 8) with CFPC.

Fig. 9 shows a box plot of the reaction force corresponding to the 30 force peaks for each control method (3 pressings for each trial; 10 trials each of CFMC and CFPC). The red line indicates the average over the 30 peaks, which shows that the reaction force on the actuator using CFMC (around 5.7 N) is around 1 N higher than that using the CFPC (around 4.7 N), equivalent to an approximate 21% increase. It is consistent with the calculation of the reaction force ($0.22MPa * \pi * (0.008/2m)^2 = 1.1N$) applied to the sensor contact area (8 mm diameter round area) due to the pressure difference ($3.5psi \approx 0.22MPa$) in Fig. 8.

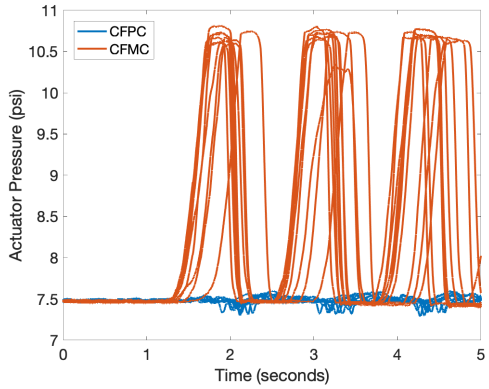

Fig. 8. Comparison of dynamic pressure range between constant fluidic mass control (CFMC) and constant fluidic pressure control (CFPC). The air source pressure is 7.5 psi.

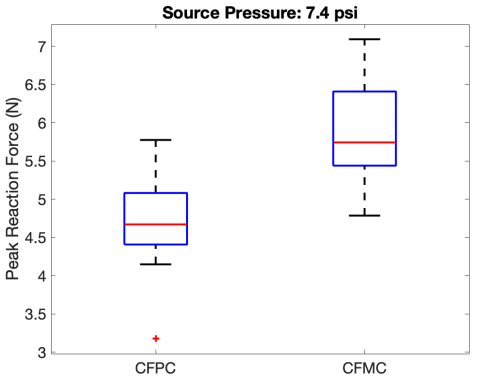

Fig. 9. Comparison of the range of peak reaction force range during dynamic interaction between constant fluidic mass control (CFMC) and constant fluidic pressure control (CFPC).

B. Experiment 2: Faster Response Time

A sample set of actuator inflation and deflation times from Experiment 2 are shown in Figs. 10 and 11, respectively. We see sharp decreases/increases (shown in the red dashed circles) in the actuator pressure, both during inflation and deflation, when the valve is turned off. The authors hypothesize that this is because the air in the blocked channel of the primary valve is mixed with the air in the actuator during the operation switch from (a) to (b) (or from (c) to (b) in the depressurizing trials) in Fig. 5.

Four key variables were considered when comparing the performance between CFMC and CFPC: the air source pressure, the initial actuator pressure, the supply/exhaust valve on-time, and the final actuator pressure. The air source pressure and the initial actuator pressure were measured by the corresponding pressure sensor before each trial. The supply/exhaust valve on-time is from the commander. The final actuator pressure is calculated by averaging the actuator pressure from 200 milliseconds to 300 milliseconds in Figs. 10 and 11.

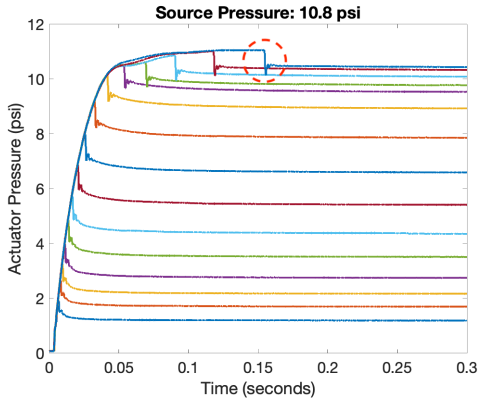

Fig. 10. Actuator pressure measurements during the pressurizing trials when the air source pressure is 10.8 psi and initial actuator pressure is ATM. The colored curves represent the trials with 15 different pressurizing times. The red dashed circle shows a sharp decrease in the actuator pressure when the valve is turned off.

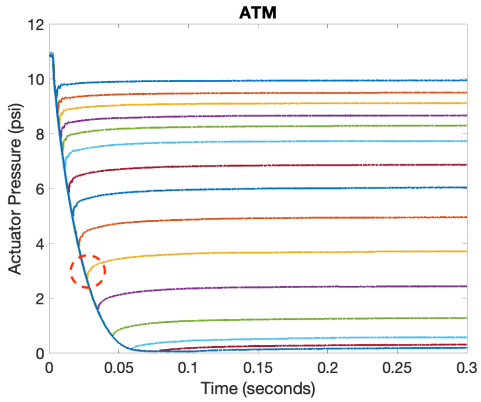

Fig. 11. Actuator pressure measurements during the depressurizing trials when the initial actuator pressure is 10.8 psi and the depressurized outlet is ATM. The colored curves represent the trials with 15 different depressurizing times. The red dashed circle shows a sharp increase in the actuator pressure when the valve is turned off.

Experimental results using 3.2, 4.7, 5.8, and 7.4 psi as the air source pressure in Experiment 1 were arbitrarily chosen to compare the response time between CFMC and CFPC, and this comparison is shown in Fig. 12. For the CFPC, the response time is the time taken by the actuator pressure to rise from ATM to 90% of the air source pressure (namely the

target pressure: 2.9, 4.2, 5.2, and 6.7 psi). For the CFMC, the response time is the pressurizing time from the commander when the final actuator pressure was equal to the target pressure. If all the final actuator pressures in Experiment 1 are not exactly equal to the target pressure, the pressurizing time is calculated by using the difference method on two adjacent times. Compared with CFPC, CFMC has a faster response time as increasing the air source pressure, even though the switches between valve operations, introduce fluctuations to the actuator pressure and the corresponding time delay.

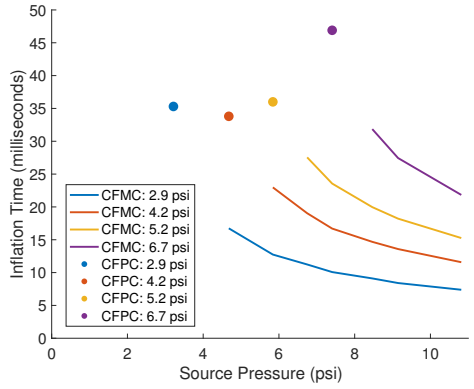

Fig. 12. Comparison of response time between constant fluidic mass control (CFMC) and constant fluidic pressure control (CFPC). Each dot represents the CFPC measurement; each curve represents the CFMC measurements. The dot and curve with the same color have the same target of the actuator pressure.

C. Experiment 2: Analog Pressure Control

For the CFPC, the actuator pressure is consistent with the air source pressure, although small fluctuations in pressure were observed under load. However, the CFMC can modulate actuator pressure continuously by adjusting the supply/exhaust valve on-time, based on the given initial actuator pressure and the air source pressure (Fig. 13).

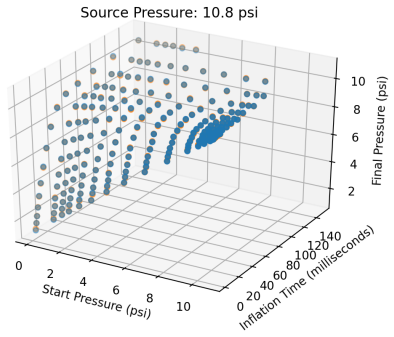

Fig. 13. Actuator pressure as a function of initial actuator pressure (namely start pressure) and pressurizing time (namely inflation time).

D. Feed-forward Neural Network: Parameter Selection

1) Number of Neurons in the Hidden Layer: Fig. 14 shows the relation between the number of neurons in the hidden layer and the training/testing error. The error continues to decrease as the number of neurons were increased from 3 to 33 and increases sharply after the number of neurons were increased to 35. This suggests that beyond 33 neurons the model has become complex enough with too many unknowns to be reasonably fit with the dataset we collected. While considering the computation cost and the error trend, a total of 10 neurons is the optimal value for our application.

2) Maximum Number of Epochs: Fig. 15 shows the relation between the number of epochs and the sum of squared error for the training set. Based on the required precision and time cost of the training process, we chose the maximum number of epochs to be one million.

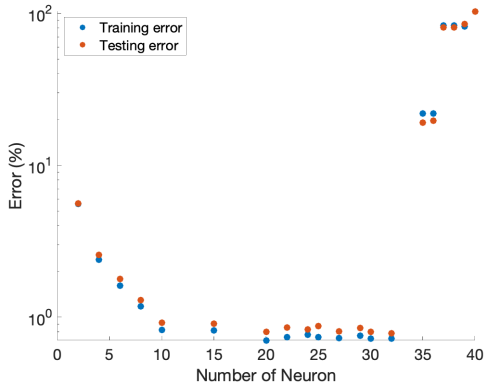

Fig. 14. The relation between the number of neurons in the hidden layer and the training/testing error.

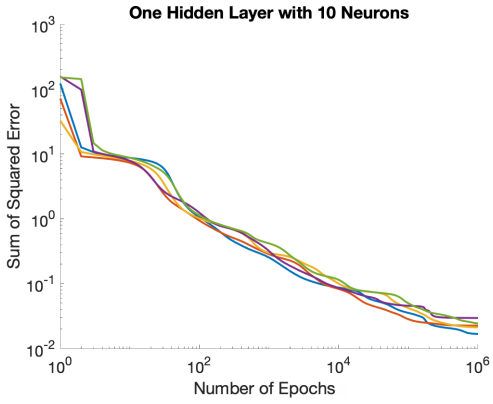

Fig. 15. The relation between the number of epochs and the sum of squared error. Each curve represents one cross-validation.

E. Feed-forward Neural Network: Performance

1) Actuator Pressure as a Function of Pressurizing/Depressurizing Time: The air source pressure and the depressurized outlet was chosen as 10.8 psi and ATM, respectively. The experimental measurements are almost overlapping the model predictions, indicating a good ability in predicting the

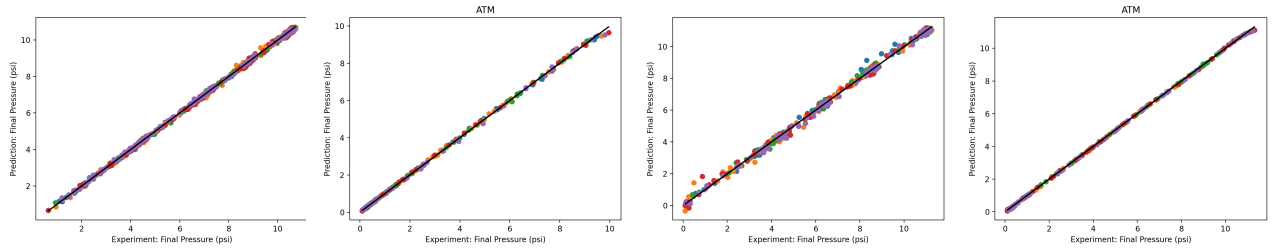

(a) (b) (c) (d)

Fig. 16. Relation between experiment measurements and Neural network predictions for the actuators under four different conditions. Each colored dataset represents one cross-validation. Figs. (a) and (b) are reuslts from the actuator with a small capacitance in Fig. 6(a). Figs. (c) and (d) are reuslts from the actuator with a large capacitance in Fig. 6(b). (a) when the air source pressure, the initial actuator pressure, and the pressurizing time are input variables; (b) when the initial actuator pressure and the depressurizing time are the input variables; (c) when the air source pressure, the initial actuator pressure, and the pressurizing time are input variables; and, (d) when the initial actuator pressure and the depressurizing time are the input variables.

actuator pressure during the pressurizing and depressurizing processes (error: 0.11% +/- 0.81%; error: 0.19% +/- 1.02%).

2) Actuator Pressure as a Function of Air Source Pressure, Initial Actuator Pressure, and Pressurizing Time: The cross-validation results from neural network model predictions based on the air source pressure, the initial actuator pressure, and the pressurizing time are shown in Fig. 16(a). The results show that the neural network algorithm can predict the actuator pressure precisely under different air source pressures, initial actuator pressures, and pressurizing time (error in Fig. 16(a): 0.84% +/- 1.41%; error in Fig. 16(b): 0.93% +/- 1.76%).

3) Actuator Pressure as a Function of Initial Actuator Pressure, and Pressurizing/Depressurizing Time: Since the function above is in four-dimensional space, it is difficult to visualize the results using a single plot. To show the comparison between the experiment measurements and the model predictions, the neural network algorithms in this function are represented as 3D surfaces for the pressurizing and depressurizing process, respectively (error: 0.62% +/- 1.17%; error: 0.94% +/- 1.24%). Based on this algorithm, we could achieve the analog control of the actuator pressure with high precision.

F. Neural Network Approach: Generalization

Figs. 16(c) and 16(d) shows that our approach has a good ability to predict the actuator pressure even though the capacitance of the soft actuator changes significantly during the pressurizing process. Additionally, these two figures also confirm that the actuator-specific learned neural network can precisely control the actuator pressure and our approach can be easily generalized.

V. Discussion

Our approach offers the following advantages and addresses the limitations of CFPC control:

1) Larger dynamic range: Since CFMC approach traps a constant mass of air inside the actuator, any interaction with the actuator, which reduces the actuator volume, results in increase in actuator pressure. This increase in pressure results in an increase in actuator impedance and therefore, increases the range of forces that the actuator can render during a haptic interaction.

2) Faster actuator response: In CFMC, a much higher source pressure can be used than what the actuator can handle by modulating the time for which the valve is turned on. By using a source pressure much higher than required, a much faster actuator inflation response is achievable to reach the same actuator pressure. A fast actuator deflation response is also possible by using vacuum at the valve exhaust.

3) Analog pressure control: In CFMC, the on-time of the valve determines the final pressure reached inside the actuator. So, by modulating the on-time of the valve, the actuator can be inflated to different pressures. An open-loop control of pressure can be achieved by implementing a pressure observer that uses a learned actuator-specific model. More accurate closed-loop control of pressure can also be achieved by deploying a soft pressure sensor within the actuator.

4) Natural haptic interaction: The increase in impedance of the actuator as the user interacts with it is important to provide the illusion of object stiffness, which is non-existent in CFPC. Furthermore, since this increase in impedance is tied to when the user interacts with the actuator (reactive or endogenous) rather than actuator pushing on the finger when inflated (active or exogenous), this type of control feels more natural than CFPC.

Although we demonstrated the accuracy of our neural network approach in two different soft TPU-fabric actuators which cover a wide range of capacitances we would see in most haptics applications, we haven't tested for all nonlinearities possible in capacitance. More variables of the actuators (such as bladder size, materials) and the fluidic system (such as material and design parameters of the fluidic tubings) are required to be considered in a comprehensive generalization analysis. However, with our neural network architecture, we should be able to capture more complex nonlinearities with increasing complex networks. Furthermore, though use of a neural network makes our approach more complex for real-time robotic systems, there are numerous examples of neural-network-based real-time robotic systems, and learned controllers are increasingly being used to achieve more

sophisticated behavior in such systems [19]. Neural networks are computationally expensive to train offline, but once the model is trained the actual prediction based on the learned model is fast and can be easily executed in a real-time manner.

This study has demonstrated multiple advantages of CFMC over CFPC, but these come at the cost of additional control infrastructure. To precisely control the actuator air the pressure control there is the need for additional equipment, with the additional valve and pressure sensors, and a more complex control strategy is required. In addition, since the CFMC enables a larger dynamic range, this requires the soft actuators to be designed to handle a larger range of pressures.

VI. Conclusion and Future Work

In this work, we present a new control method for soft fluidic actuators, CFMC, which uses an arrangement of two valves to maintain a constant fluidic mass within the actuator, that has potential advantages in wearable haptics. Our analyses show that compared to CFPC, CFMC results in a higher dynamic range of actuator output forces and faster response time for inflation and deflation. In addition, we demonstrated an implementation of analog pressure control based on CFMC using a learned neural-network-based algorithm, which enabled us to accurately modulate the actuator pressure. Furthermore, experiments showed that our approach can be generalized to different soft TPU-fabric fluidic actuators.

The external interaction force on the soft actuator is a common scenario in wearable haptics applications, and the different forces acting on the actuator can impact its equivalent capacitance, thus reducing the accuracy of the learned neural network model. In the future, we plan to extend the proposed neural network model by introducing the preload as a fourth input-variable, and explore architecture of recurrent neural networks to include input-variables with temporal dynamic behavior, such as users' behavior of soft actuators, in the control system. Furthermore, we plan to explore CFMC-based analog pressure control for a wearable haptic device. In addition, we plan to examine the impact of CFMC in creating haptic sensation of stiffness and also performance of closed-loop control.

References

[1] P. Polygerinos, Z. Wang, K. C. Galloway, R. J. Wood, and C. J. Walsh, "Soft robotic glove for combined assistance and at-home rehabilitation," *Robotics and Autonomous Systems*, vol. 73, pp. 135–143, 2015.

[2] E. Acome, S. Mitchell, T. Morrissey, M. Emmett, C. Benjamin, M. King, M. Radakovitz, and C. Keplinger, "Hydraulically amplified self-healing electrostatic actuators with muscle-like performance," *Science*, vol. 359, no. 6371, pp. 61–65, 2018.

[3] T. N. Do, H. Phan, T.-Q. Nguyen, and Y. Visell, "Miniature soft electromagnetic actuators for robotic applications," *Advanced Functional Materials*, vol. 28, no. 18, p. 1800244, 2018.

[4] S. Taccola, F. Greco, E. Sinibaldi, A. Mondini, B. Mazzolai, and V. Mattoli, "Toward a new generation of electrically controllable hygromorphic soft actuators," *Advanced Materials*, vol. 27, no. 10, pp. 1668–1675, 2015.

[5] E. M. Young, A. H. Memar, P. Agarwal, and N. Colonnese, "Bellowband: a pneumatic wristband for delivering local pressure and vibration," in *2019 IEEE World Haptics Conference (WHC)*. IEEE, 2019, pp. 55–60.

[6] M. Zhu, A. H. Memar, A. Gupta, M. Samad, P. Agarwal, Y. Visell, S. J. Keller, and N. Colonnese, "Pneusleeve: In-fabric multimodal actuation and sensing in a soft, compact, and expressive haptic sleeve," in *Proceedings of the 2020 CHI Conference on Human Factors in Computing Systems*, 2020, pp. 1–12.

[7] I. M. Koo, K. Jung, J. C. Koo, J.-D. Nam, Y. K. Lee, and H. R. Choi, "Development of soft-actuator-based wearable tactile display," *IEEE Transactions on Robotics*, vol. 24, no. 3, pp. 549–558, 2008.

[8] Y. Tanaka, H. Yamauchi, and K. Amemiya, "Wearable haptic display for immersive virtual environment," in *Proceedings of the jfps international symposium on fluid power*, vol. 2002, no. 5-2. The Japan Fluid Power System Society, 2002, pp. 309–314.

[9] A. Delazio, K. Nakagaki, R. L. Klatzky, S. E. Hudson, J. F. Lehman, and A. P. Sample, "Force jacket: Pneumatically-actuated jacket for embodied haptic experiences," in *Proceedings of the 2018 CHI Conference on Human Factors in Computing Systems*, 2018, pp. 1–12.

[10] M. Raitor, J. M. Walker, A. M. Okamura, and H. Culbertson, "Wrap: Wearable, restricted-aperture pneumatics for haptic guidance," in *2017 IEEE International Conference on Robotics and Automation (ICRA)*. IEEE, 2017, pp. 427–432.

[11] S. Kanjanapas, C. M. Nunez, S. R. Williams, A. M. Okamura, and M. Luo, "Design and analysis of pneumatic 2-dof soft haptic devices for shear display," *IEEE Robotics and Automation Letters*, vol. 4, no. 2, pp. 1365–1371, 2019.

[12] R. Deimel, M. Radke, and O. Brock, "Mass control of pneumatic soft continuum actuators with commodity components," in *2016 IEEE/RSJ International Conference on Intelligent Robots and Systems (IROS)*. IEEE, 2016, pp. 774–779.

[13] R. W. Colbrunn, G. M. Nelson, and R. D. Quinn, "Modeling of braided pneumatic actuators for robotic control," in *Proceedings 2001 IEEE/RSJ International Conference on Intelligent Robots and Systems. Expanding the Societal Role of Robotics in the the Next Millennium (Cat. No. 01CH37180)*, vol. 4. IEEE, 2001, pp. 1964–1970.

[14] P. Polygerinos, Z. Wang, J. T. Overvelde, K. C. Galloway, R. J. Wood, K. Bertoldi, and C. J. Walsh, "Modeling of soft fiber-reinforced bending actuators," *IEEE Transactions on Robotics*, vol. 31, no. 3, pp. 778–789, 2015.

[15] A. A. Stanley, A. Amini, C. Glick, N. Usevitch, Y. Mengüç, and S. J. Keller, "Lumped-parameter response time models for pneumatic circuit dynamics," *Journal of Dynamic Systems, Measurement, and Control*, vol. 143, no. 5, 2021.

[16] Y. Kim, B. Kuczenski, P. R. LeDuc, and W. C. Messner, "Modulation of fluidic resistance and capacitance for long-term, high-speed feedback control of a microfluidic interface," *Lab on a Chip*, vol. 9, no. 17, pp. 2603–2609, 2009.

[17] A. Russomanno, R. B. Gillespie, S. OModhrain, and J. Barber, "Modeling pneumatic actuators for a refreshable tactile display," in *International Conference on Human Haptic Sensing and Touch Enabled Computer Applications*. Springer, 2014, pp. 385–393.

[18] M. Giorelli, F. Renda, M. Calisti, A. Arienti, G. Ferri, and C. Laschi, "Neural network and jacobian method for solving the inverse statics of a cable-driven soft arm with nonconstant curvature," *IEEE Transactions on Robotics*, vol. 31, no. 4, pp. 823–834, 2015.

[19] G. A. Bekey and K. Y. Goldberg, *Neural networks in robotics*. Springer Science & Business Media, 2012, vol. 202.